

All-Weather Droplet-Based Triboelectric Nanogenerator for Wave Energy Harvesting

Xuelian Wei,[▽] Zhihao Zhao,[▽] Chuguo Zhang,[▽] Wei Yuan, Zhiyi Wu,^{*} Jie Wang,^{*} and Zhong Lin Wang^{*}



Cite This: <https://doi.org/10.1021/acsnano.1c02790>



Read Online

ACCESS |



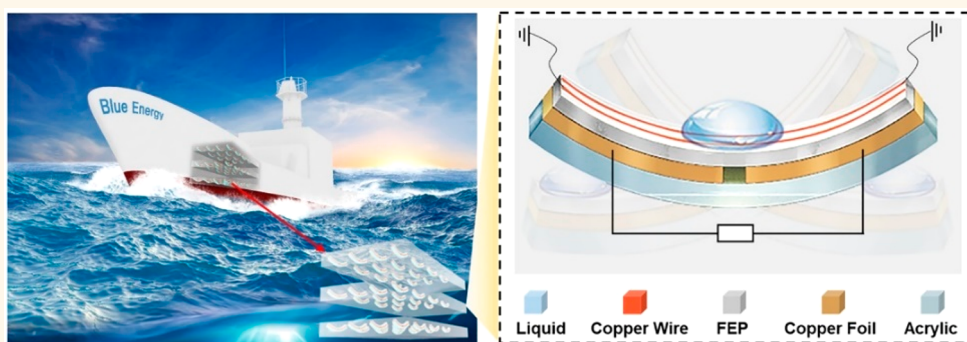
Metrics & More



Article Recommendations



Supporting Information



ABSTRACT: The liquid–solid triboelectric nanogenerator (LS-TENG) has been demonstrated to harvest energy efficiently through the contact electrification effect between liquid and solid triboelectric materials, which can avoid the wear issue in solid–solid TENG. However, the droplet-based LS-TENG reveals the problems that it generally works with the continuous falling droplets or needs to be fully packaged, which greatly limit its practical application. Here, a droplet-based triboelectric nanogenerator (DB-TENG) with a simple open structure is designed to effectively solve these problems. The nonpackaged DB-TENG can work stably under extreme conditions with high humidity or high concentrations of salt, acid, or alkali solutions, showing the DB-TENGs can be flexibly utilized in all types of working environments with better reliability and lower maintenance costs. It is of great significance that the integrated DB-TENG network array can realize the all-weather ocean energy harvesting. Furthermore, under the simulated ocean wave, a scaled-up DB-TENG with considerable output performance can charge capacitors and drive electrical devices. Overall, the DB-TENG shows many advantages: simple open structure, all-weather working ability, timely supplement of water loss, no tight packaging, wear resistance, suitable for extreme working environments. This work provides a convenient and feasible way toward all-weather wave energy harvesting in real marine environments.

KEYWORDS: liquid–solid triboelectric nanogenerator, all-weather, wave energy harvesting, blue energy, triboelectrification effect

Seventy percent of the Earth's surface is covered by oceans, which contains abundant and renewable energy. Thus, it has become an inevitable trend for mankind to harvest energy from the ocean.^{1–3} Sea waves represent one of the universal motions formed on the ocean, and its corresponding energy is also one of the richest energy in the ocean,^{4,5} but how to efficiently harvest the low-frequency wave energy is an urgent problem to be solved. The electromagnetic generator is the main method to harvest wave energy; however, it is greatly limited by its high cost and heavy weight, as well as the unsuitability for harvesting low-frequency energy.^{3,6–8}

As a next generation of energy harvesting technology, triboelectric nanogenerator (TENG)-based wave energy

harvester has caught much attention for its particular advantages, such as simple structure, lightweight, low cost, and diverse selection of friction materials.^{9–16} In particular, the excellent capability of TENG to harvest the low-frequency energy makes it suitable for ocean energy harvesting.¹⁷ The

Received: April 1, 2021

Accepted: July 27, 2021

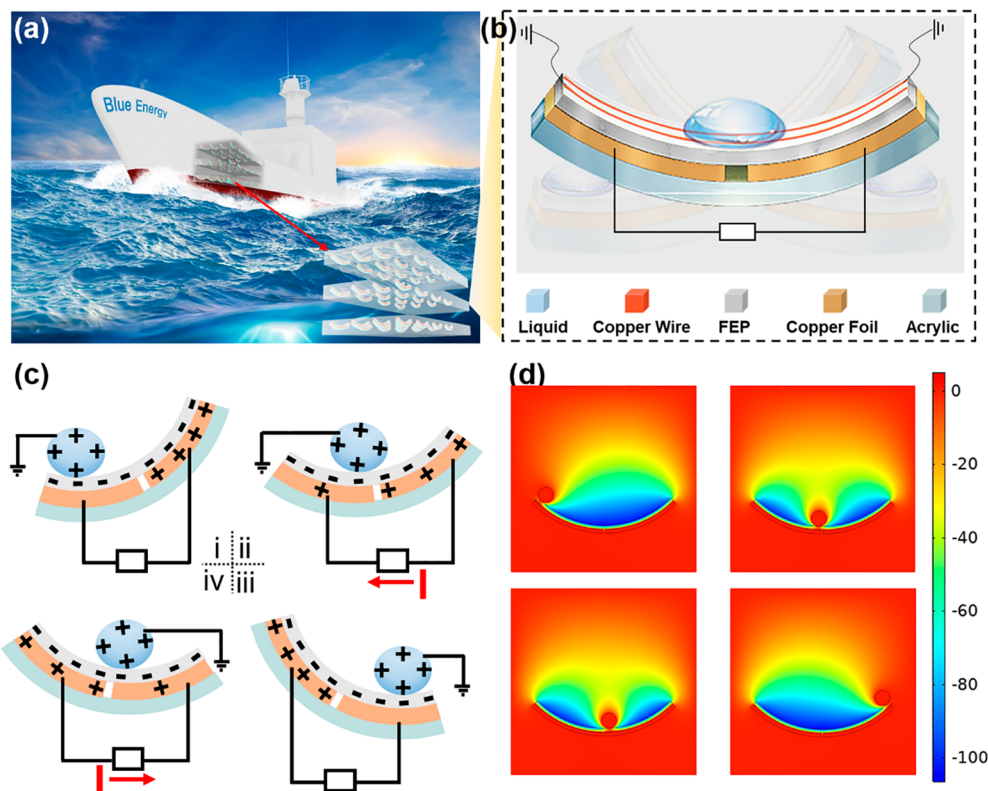


Figure 1. Structural design and working mechanism of DB-TENG. (a) Structural diagram of DB-TENG arrays on the deck of a model ship of Blue Energy. (b) The enlarged view of the DB-TENG unit. (c) Working mechanism of the DB-TENG and (d) the corresponding simulated potential distribution.

traditional research of TENG-based blue energy harvesters is based on the triboelectrification effect between solid with solid and electrostatic induction effect due to the high performance of solid–solid triboelectric nanogenerator (SS-TENG).^{18–23} However, the SS-TENG always presents two inevitable problems when it is utilized as a blue energy harvester. The first one is the durability of the friction materials: the serious wear problems will degrade the output performance and operation life of the TENG.^{24–27} The second is the packaging problem of the TENG devices: high humidity and extreme working conditions will decrease the output of TENG.^{25,28} Whereas, the liquid–solid contact triboelectric nanogenerator (LS-TENG) can effectively avoid these problems, as well as its high instantaneous output and energy conversion efficiency,^{29–34} showing tremendous potential for blue energy harvesting. Besides, the LS-TENG has been extended to the self-powered sensor with high sensitivity and excellent stability.³⁵ However, the droplet-based LS-TENG generally works with continuous falling droplets³⁶ or needs to be fully packaged.^{35,37} Moreover, although full packaging structure can solve the influence of humidity on the triboelectric performance, it cannot avoid the adverse effect of dielectric shielding from the water.^{38,39} Therefore, it is necessary to achieve a higher output performance LS-TENG and operate continuously under all working conditions.

Here, a droplet-based triboelectric nanogenerator (DB-TENG) with simple open-structure is designed to effectively overcome the functional discontinuity of previous droplet-based LS-TENG energy harvesters, which can only work in the rainy condition. A high surface charge density of $153.5 \mu\text{C m}^{-2}$ can be realized with the fluorinated ethylene propylene (FEP)

films and deionized water (DI) droplets as friction materials, which is higher than the value of a large part of SS-TENGs. The DB-TENG can also work stably in a variety of extreme environments, such as high humidity and high concentrations of salt solutions, strong acids or alkalis, which greatly reduces the difficulty of device packaging. It is of great significance that the integrated DB-TENG network array can realize the all-weather ocean energy harvesting. Furthermore, under the simulated ocean wave, a nonpackaged scaled-up DB-TENG with considerable output performance can charge capacitors or drive electronic devices. In all, the all-weather DB-TENG provides a practical strategy for the collection of ocean energy in real ocean environments.

RESULTS AND DISCUSSION

Structure Design and Working Principle. A vessel is used as a platform, which provides obvious advantages for wave energy harvesting, because of its special movement form in water, stable and large enough internal space, and the electrostatic shielding characteristic of ship hull.⁴⁰ The DB-TENG arrays with simple open structure and low cost can be installed on the ship to harvest the wave energy with the shaking of the ship (Figure 1a). The schematic diagram of single DB-TENG is shown in Figure 1b. A thin FEP film is used as the dielectric film and two separate symmetrical copper electrodes are plated on the back of the film. The detailed production process is shown in the Experimental Section. It is important to note that there are two thin copper wires on the upper surface of the dielectric film to ground the droplet constantly. Through testing, we demonstrate that the grounding connection mode leads to higher output perform-

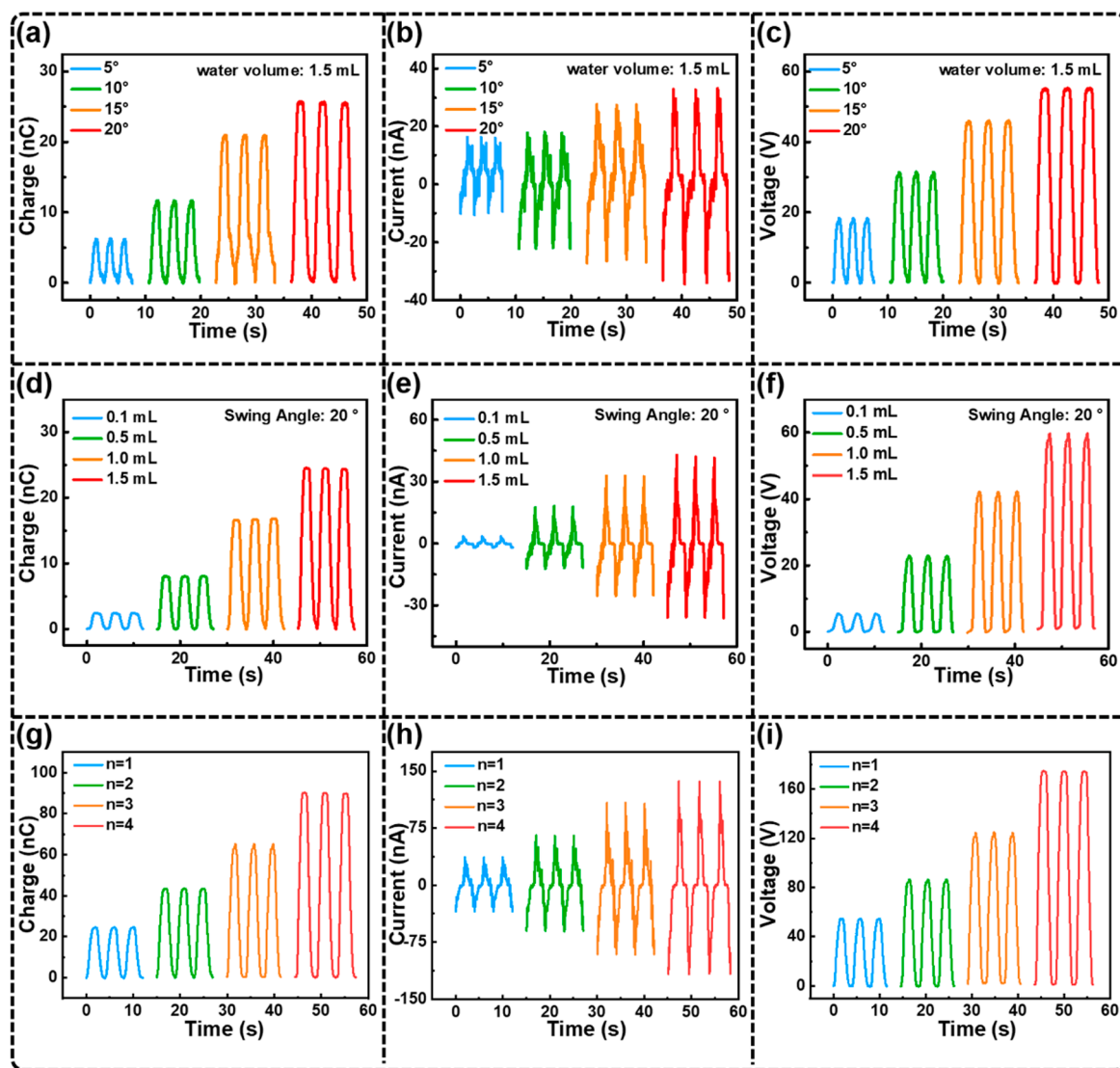


Figure 2. Output performance of the DB-TENG under different influencing factors: (a) transferred charges, (b) short-circuit current, and (c) open-circuit voltage of the DB-TENG under different swing angles; (d) transferred charges, (e) short-circuit current, and (f) open-circuit voltage with increasing droplet volume. (g–i) The relationship between the number of DB-TENG units ($n = 1, 2, 3, 4$) and output performance.

ance than the ungrounded one (see Figure S1 in the Supporting Information). The possible reason is that the potential at the interface between the grounded droplet and the film is lower than in the ungrounded connection, which is favorable for the electrostatic induction. The details of the mechanism are needed to further study in the future work. The simulation results of the ungrounded support this speculation (Figure S2 in the Supporting Information) and explanation of the simulated potential distribution diagram of the ungrounded connection can be obtained in Note S1 in the Supporting Information. The schematic diagram of two wiring modes and the experimental test device is shown in Figures S3 and S4 in the Supporting Information. The DB-TENG is the free-standing triboelectric-layer mode, which is based on the coupling of triboelectrification effect and electrostatic induction effect.⁴¹ Although the surface charge of water is almost unanimously accepted to have a negative sign,⁴² positive triboelectric charges will be generated on the droplet after direct contact with the surface of FEP.^{43,44} It can also be verified by a comparative experiment, as shown in Figure S5 in

the Supporting Information (see Note S2 in the Supporting Information for discussion). The specific transfer mechanism in the contact process between droplets and films, whether electron transfer,⁴⁵ ion transfer,⁴⁶ or other transfer mechanism,⁴⁷ is still unclear and inconclusive. But anyway, it is undisputed that the charge transfer process on the back electrode (copper electrode) of the negatively charged FEP film after contacting with droplets. Figure 1c(i) shows the electrical characterization of a droplet at an initial position. When the droplet slides from the left electrode to the middle part, the electrons will flow from the left electrode to the right electrode through an external circuit, because of the electrostatic induction effect (Figure 1c(ii)). When the droplet reaches the spot where it coincides with the right electrode, as shown in Figure 1c(iii), all the electrons will flow to the right electrode. Subsequently, since the droplet slides back (Figure 1c(iv)), the electrons will transfer from the right electrode to the left electrode through an external circuit and generate a reverse current. These working mechanisms are confirmed with the potential distribution of droplets at four different

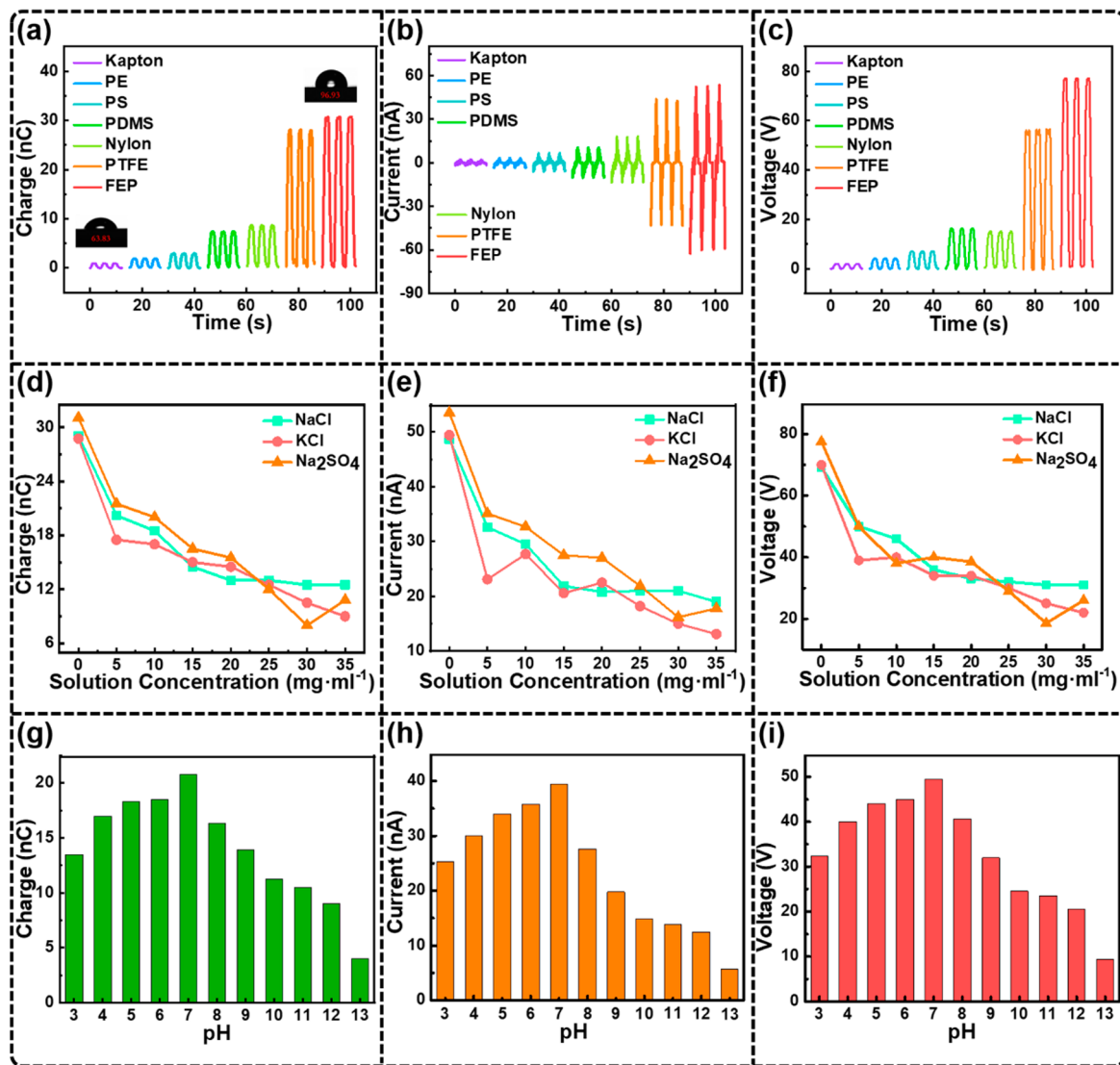


Figure 3. Output performance of DB-TENG with different triboelectric materials: (a) the transferred charges, (b) short-circuit current, and (c) open-circuit voltage of the DB-TENG with different dielectric films (the inset shows DI water contact angles of different dielectric film); (d) the transferred charges, (e) short-circuit current, and (f) open-circuit voltage of the DB-TENG based on droplet with different concentrations of salt solutions; (g) the transferred charges, (h) short-circuit current, and (i) open-circuit voltage of the DB-TENG based on droplet with various pHs.

positions by finite-element analysis (COMSOL Multiphysics), as shown in Figure 1d, and the simulated potential distribution of droplet sliding process can be referred to Movie S1 in the Supporting Information.

Output Performance of DB-TENG. The output performance of DB-TENG under different influencing factors is shown in Figure 2. For a certain water volume, it is clear that the transfer charge (Q_{tr}), the short-circuit current (I_{sc}), and the open-circuit voltage (V_{oc}) gradually increase from 6.0 nC to 27.0 nC, 16.0 nA to 34.5 nA, and 19.0 V to 56.1 V when the swing angle increases from 5° to 20° (Figures 2a–c), respectively. Similarly, the output performance of DB-TENG keeps an increased linear relationship with water volume increasing at the fixed angle of swing (20°), as shown in Figure 2d–f. When the water volume reaches to 1.5 mL, the contact areas were calculated to be $S = 2 \text{ cm}^2$ (see Note S3 in the Supporting Information for detail regarding the calculation process), the output performance reaches maximum ($Q_{tr} = 24.4 \text{ nC}$, $I_{sc} = 40.0 \text{ nA}$, and $V_{oc} = 58.0 \text{ V}$). The water volume

exceeding 1.5 mL will lead to a decrease in the results (see Figure S6 in the Supporting Information). The water volume and the swing angle are always 1.5 mL and 20° in the subsequent experiments for convenient description, unless otherwise specified. Meanwhile, the different output performance of DB-TENG with different angular accelerations of 4–20 rad s^{-2} is shown in Figure S7 in the Supporting Information. The V_{oc} and Q_{tr} decrease simultaneously with the increase of angular acceleration. It can be seen from the pictures of droplet status at different angular accelerations (Figure S8 in the Supporting Information) that the shape of the droplet gradually changes from the teardrop shape at 4 rad s^{-2} to the flattened shape at 20 rad s^{-2} . Meanwhile, the output Q_{tr} and V_{oc} decrease as the angular acceleration increases, because of the deformation of the droplet, which decreases the effective contact area during the operating process.

To better apply to harvest ocean energy, the large-scale integration of multiple DB-TENG units is essential. The output of integration of different units is shown in Figures 2g–

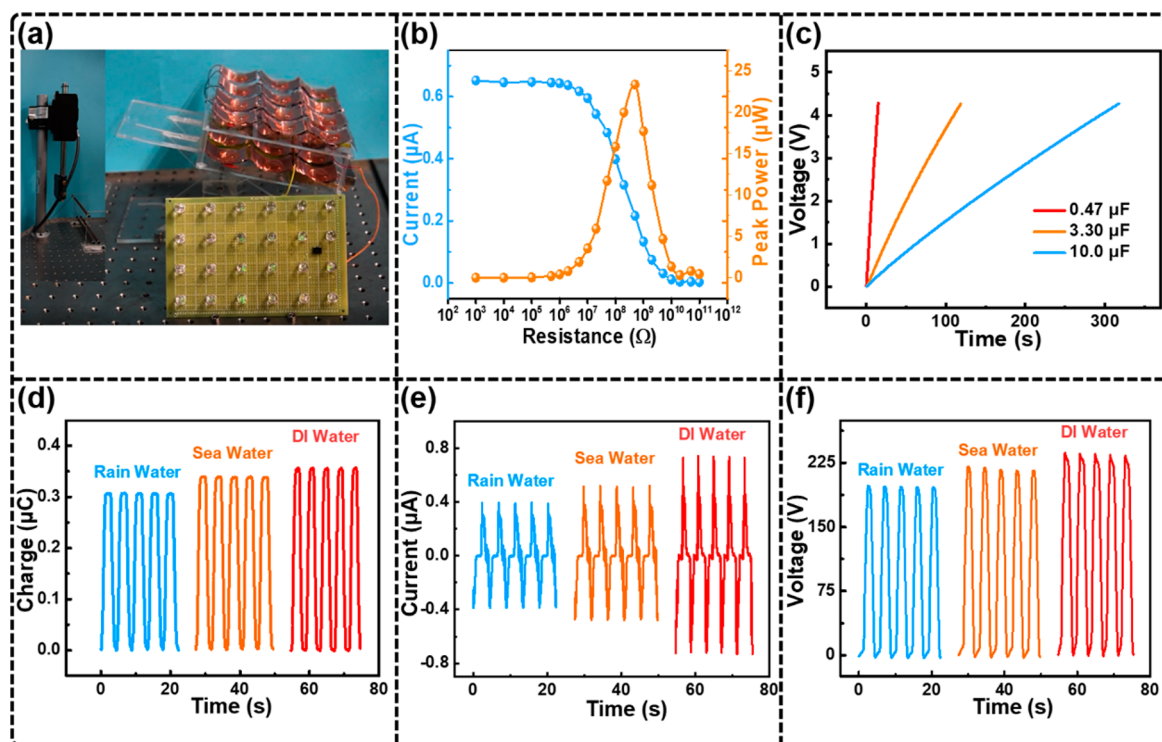


Figure 4. Application of the integrated DB-TENG. (a) Photograph of the multidevice integrated DB-TENG array and the entire test system. (b) The output current and the peak power of the integrated device under different loads. (c) The charging curves of the integrated device for different capacitors. (d) The transferred charges, (e) short-circuit current, and (f) open-circuit voltage of the integrated DB-TENG with three practical application scenarios.

i. It can be clearly seen that the values of Q_{tr} , I_{sc} , and V_{oc} increase linearly as the number of DB-TENG units increases; furthermore, more DB-TENG units can be integrated to achieve large-scale energy harvesting.

Effects of Triboelectric Materials. The output performance of DB-TENG with different triboelectric materials is demonstrated in Figures 3a–c. We can find that the specie of triboelectric material affects the output charge density significantly. The FEP film shows best output performance ($Q_{tr} = 30.7$ nC, $I_{sc} = 52.0$ nA, and $V_{oc} = 77.0$ V), and the surface charge density (based on the area of tater droplet⁴⁸) is calculated to be $153.5 \mu\text{C m}^{-2}$ (Note S3), but the Kapton film presents the worst one ($Q_{tr} = 1.0$ nC, $I_{sc} = 2.4$ nA, and $V_{oc} = 2.1$ V), and the charge density is only $5.1 \mu\text{C m}^{-2}$. Figure S9 in the Supporting Information presents a comparison of the surface charge densities reported in recent years, it can be seen that the charge density of this work has the highest result.^{38,43,49,50} The results are mainly related to electron affinity, ionization energy, and surface hydrophobicity of different triboelectric materials (see Note S4 in the Supporting Information).^{37,46,51,52} The wetting property of different triboelectric films is investigated by water contact angle measurement, as shown in Figure S10 in the Supporting Information. The FEP film has the highest output performance, because of its greater ability to acquire electrons and better surface hydrophobicity. The output performance of Kapton is not optimistic, because of its poor hydrophobicity. On the other hand, the triboelectrification effect of different films also shows a close relationship with the output performance of different triboelectric materials, for example, the PDMS shows an excellent hydrophobicity, but it provides a weak output, because of its poor triboelectrification effect with

water.⁵³ To determine the output performance of DB-TENG in different solution environments, salt solutions containing different ions and aqueous solutions with different pHs were used for multiple experiments. Figures 3d–f show the output performance of DB-TENG, whose droplets have different concentrations of salt solution (triboelectric materials: FEP film). Obviously, the Q_{tr} , I_{sc} , and V_{oc} values decrease from 29.0 nC to 12.5 nC, 48.7 nA to 19.0 nA, and 69.2 to 31.0 V, respectively, with the increase of the concentration of NaCl from 0 to 35 mg mL⁻¹. A similar trend is revealed in the DB-TENG whose droplets is the different concentration solution of KCl and Na₂SO₄, indicating that salt solution will lead to a significant reduction of the electric output.^{29,33,54} In addition, the effects of droplets with different pHs on the output performances of DB-TENG are shown in Figures 3g–i. The droplets with different pHs are the aqueous solutions with certain concentration of HCl and NaOH. In an acidic environment (pH < 7), with pH increasing, the Q_{tr} increased gradually from 13.5 nC at pH 3 to 18.5 nC at pH 6. In an alkaline environment (pH > 7), the Q_{tr} increases from 4.0 nC at pH 13 to 16.3 nC at pH 8 with decreasing pH. However, the highest electric output of the DB-TENG is achieved in a neutral environment, namely pH = 7, confirming the results in Figures 3d–f that the output performance is the maximum when the salt solution concentration is 0 (deionized water), which can be attributed to the weak screen effect of fewer free ions (H⁺ ions, Na⁺ ions).⁴³

Application of the Integrated DB-TENG. To further measure practical application of the DB-TENG, we fabricated an integrated array with 24 DB-TENGs, as shown in Figure 4a. More than two dozen commercial LEDs can be lit simultaneously, using DI water droplets (see Movie S2 in the

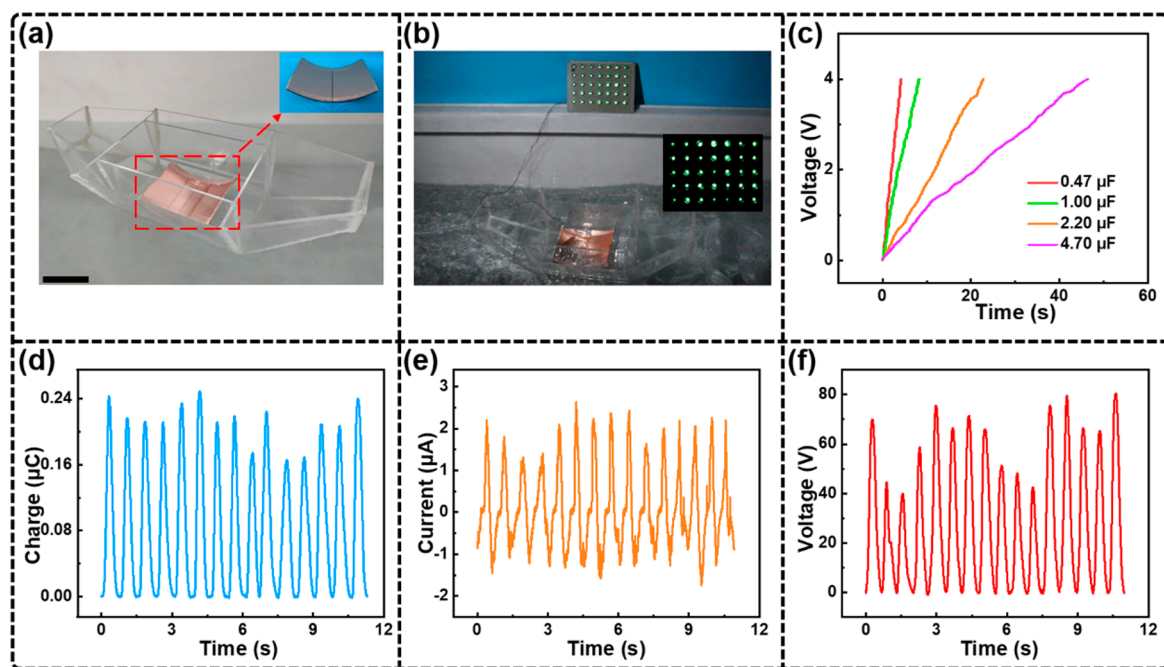


Figure 5. Output performance in simulated ocean waves. (a) Photograph of the scaled-up DB-TENG on a test ship (scale bar, 6 cm), the inset is a photograph of an actual test device. (b) Demonstrations of the DB-TENG as a power source to light the LEDs in water tank (inset: lighting condition in the dark). (c) The charging curves of the scaled-up DB-TENG for different capacitors. (d) Transferred charges, (e) short-circuit current, and (f) open-circuit voltage of a scaled-up droplet-based TENG in simulated ocean waves.

Supporting Information). In addition, as shown in Figure 4b, as well as Figure S11 in the Supporting Information, the amplitude of the voltage increases with the increase in external resistance, while the current is in a completely opposite trend. The output peak power can reach $23.3 \mu\text{W}$ when the load resistance is $500 \text{ M}\Omega$. Figure 4c depicts the charging curves of different capacitors (0.47 , 3.3 , and $10 \mu\text{F}$) charged by the integrated DB-TENG array at an angular acceleration of 4 rad s^{-2} (simplified circuit diagram is depicted in Figure S12 in the Supporting Information), where the $0.47 \mu\text{F}$ capacitor can be instantly charged to 4.0 V within 14 s . In order to better study and apply the integrated DB-TENG array in different environments and climates in the ocean, the output performance of three different solutions is tested in the laboratory (Figures 4d–f). The output performance of a single DB-TENG with three different droplets is shown in Figure S13 in the Supporting Information. For droplets of deionized water, the Q_{tr} , I_{sc} and V_{oc} of the multidevice integrated array can reach to 360.0 nC , 746.0 nA , and 237.0 V , respectively. It can be seen that, although the Q_{tr} , I_{sc} , and V_{oc} of rainwater and seawater are only slightly lower than that of DI water, which is of great significance for all-weather ocean energy harvesters. The DB-TENG provides a more-practical open structure for all-weather wave energy harvesting in a real marine environment.

To demonstrate the wave energy harvesting performance of the DB-TENG, a scaled-up DB-TENG was fixed on a ship to ensure that the harvester moves along with the ship's motion, and placed together in a water tank to simulate ocean waves (Figure 5a). The inset shows a photograph of such large-size testing device (Figure 5a). The diagram of the scaled-up DB-TENG swinging state with a ship is shown in Figure S14 in the Supporting Information. Under the simulated ocean wave, the scaled-up DB-TENG can be used as a practical electric energy supply source to drive 35 green light LEDs (rated power, 45 mW), as shown in Figure 5b, as well as Movie S3 in the

Supporting Information. Because of the characteristics of the AC output of the TENG and the difference in the amplitude of the simulated ocean waves shaking, the LEDs blink alternately and the brightness is different every time. As an energy harvester, the wave energy harvesting by DB-TENG can also be stored in capacitors for the subsequent utilization. Figure 5c shows the charging curves of different capacitors charged by the scaled-up DB-TENG in simulated ocean waves, and the detailed circuit is shown in Figure S12 in the Supporting Information. A $0.47 \mu\text{F}$ capacitor can be charged to $\sim 4 \text{ V}$ within 4.1 s . As shown in Figures 5d–f, the Q_{tr} , I_{sc} and V_{oc} of the scaled-up DB-TENG is $\sim 0.2 \mu\text{C}$, $\sim 2.5 \mu\text{A}$, and $\sim 70 \text{ V}$, respectively. It is shown that this simple open structure has observable output performance and practical application capability, and it can be used for large-scale ocean energy harvesting.

CONCLUSION

In summary, an all-weather droplet-based triboelectric nanogenerator (DB-TENG) with simple structure is fabricated to efficiently harvest wave energy from ocean. The Q_{tr} , I_{sc} and V_{oc} driven by a mere 1.5 mL droplet can reach 30.7 nC , 52.0 nA , and 77.0 V (surface charge density: $153.5 \mu\text{C m}^{-2}$), respectively. The DB-TENG can work stably in a variety of extreme environments, such as high concentrations of salt solutions, strong acids or alkalis, which greatly reduces the difficulty of device packaging. It is of great significance that an integrated array consisting of 24 DB-TENG can work well by using actual rainwater and seawater. Furthermore, under the simulated ocean wave, a scaled-up DB-TENG with a considerable output performance can charge capacitors and drive electronic devices. Relying on the simple open structure and excellent output performance in a variety of marine environments and weather conditions, DB-TENG can timely supply the water loss caused by shaking of the ship or water

evaporation in situ to maintain stable output performance, which provides an effective strategy to harvest all-weather ocean energy in real ocean environments.

EXPERIMENTAL SECTION

The Fabrication of the Droplet-Based TENG. A sliding freestanding triboelectric-layer mode TENG was adopted. As conducting layers, we put two pieces of copper films on the curved acrylic substrate as smooth as possible, and the curved surface makes droplets slide more easily. The curved substrate can easily be obtained by cutting an acrylic pipe with a diameter of 70 mm and the length of each section of the pipe is 30 mm. Next, a 30- μm -thick FEP is attached to the support substrate of the same size, which acts as the triboelectric dielectric material. In this experiment, deionized water, seawater, rainwater, and salt solutions of different concentrations were used in the laboratory research. Rain water and seawater were taken from the real environment. The DB-TENG used in the simulated ocean waves test is an enlarged sample of the above device. The substrate of this scaled-up DB-TENG is a quarter acrylic circular tube with an outside diameter of 250 mm and a length of 120 mm. The rest of the fabrication process and material selection are consistent with the above.

Electrical Measurement of the TENGs. A programmable electrometer (Model 6514, Keithley Instruments, USA) was utilized to measure the open-circuit voltage, the short-circuit current and the transfer-charge quantity of the TENGs. To simulate the wave motion, the actions of the device are successfully fulfilled with the cooperation of a vertical linear motor (PS01-37SX120F-HP-N, The LinMot, Inc., USA) and a homemade seesaw structure. A potentiostat (Biologic, VMP3, Bio-Logic Science Instruments, France) was employed to obtain the voltage signal of the capacitor in the self-charging power system. The film and its surface wetting property were observed and studied by a contact angle measurement instrument (Model CA100C, Shanghai Innuo Precision Instruments Co., Ltd).

ASSOCIATED CONTENT

Supporting Information

The Supporting Information is available free of charge at <https://pubs.acs.org/doi/10.1021/acsnano.1c02790>.

Movie S1: The simulated potential distribution of droplet sliding process using the finite-element method via the commercial software COMSOL (MP4)

Movie S2: LEDs are lit simultaneously using DI water droplets with integrated array with 24 DB-TENGs (MP4)

Movie S3: Thirty-five LED light bulbs are lighted by vessel with a scaled-up DB-TENG module in water wave (MP4)

Figures S1–S14 provide the output electrical performance of grounding and no grounding for a droplet on the FEP film; the simulated potential distribution of the ungrounded connection at four different locations; schematic diagram of two wiring modes; the structure diagram of the whole test device and shaking process; comparison of electrical characterization between steel ball and droplet after contact with FEP films; the relationship between output performance and droplet volume; output performance of the droplet-based TENG at different angular accelerations; the droplet status at different angular accelerations; comparison of the charge density reported in recent years with this work; surface contact angles of different films; the variation of current, voltage and power with external circuit resistance; circuit diagram of the self-powered system; output performance of a single DB-TENG with

three different droplets; photograph of the scaled-up DB-TENG on a test ship. Notes S1–S3 provide an explanation of the simulated potential distribution diagram of the ungrounded connection; a brief discussion of the electrical characterization of droplets contact with FEP surface; calculation of the contact area and the surface charge density (PDF)

AUTHOR INFORMATION

Corresponding Authors

Zhiyi Wu – Beijing Institute of Nanoenergy and Nanosystems, Chinese Academy of Sciences, Beijing 100083, China; College of Nanoscience and Technology, University of Chinese Academy of Sciences, Beijing 100049, People's Republic of China; Email: wuzhiyi@binn.cas.cn

Jie Wang – Beijing Institute of Nanoenergy and Nanosystems, Chinese Academy of Sciences, Beijing 100083, China; College of Nanoscience and Technology, University of Chinese Academy of Sciences, Beijing 100049, People's Republic of China; orcid.org/0000-0003-4470-6171; Email: wangjie@binn.cas.cn

Zhong Lin Wang – Beijing Institute of Nanoenergy and Nanosystems, Chinese Academy of Sciences, Beijing 100083, China; College of Nanoscience and Technology, University of Chinese Academy of Sciences, Beijing 100049, People's Republic of China; School of Materials Science and Engineering, Georgia Institute of Technology, Atlanta, Georgia 30332, United States; orcid.org/0000-0002-5530-0380; Email: zhong.wang@mse.gatech.edu

Authors

Xuelian Wei – Beijing Institute of Nanoenergy and Nanosystems, Chinese Academy of Sciences, Beijing 100083, China; College of Nanoscience and Technology, University of Chinese Academy of Sciences, Beijing 100049, People's Republic of China

Zhihao Zhao – Beijing Institute of Nanoenergy and Nanosystems, Chinese Academy of Sciences, Beijing 100083, China

Chuguo Zhang – Beijing Institute of Nanoenergy and Nanosystems, Chinese Academy of Sciences, Beijing 100083, China; College of Nanoscience and Technology, University of Chinese Academy of Sciences, Beijing 100049, People's Republic of China

Wei Yuan – Beijing Institute of Nanoenergy and Nanosystems, Chinese Academy of Sciences, Beijing 100083, China; College of Nanoscience and Technology, University of Chinese Academy of Sciences, Beijing 100049, People's Republic of China

Complete contact information is available at: <https://pubs.acs.org/doi/10.1021/acsnano.1c02790>

Author Contributions

^vThese authors contributed equally to this work.

Author Contributions

X.L.W., Z.Y.W., J.W., and Z.L.W. conceived the idea, analyzed the data, and wrote the paper. X.L.W. and C.G.Z. designed the structures of the vessel and DB-TENG. Z.H.Z. optimized the paper and modified pictures. W.Y. helped with the experiments. All the authors discussed the results and commented on the manuscript.

Notes

The authors declare no competing financial interest.

ACKNOWLEDGMENTS

This research was supported by the National Key R & D Project from Minister of Science and Technology (No. 2016YFA0202704), The Key Research Program of Frontier Sciences, Chinese Academy of Sciences (No. ZDBS-LY-DQC025), National Natural Science Foundation of China (Grant Nos. 61774016, 5151101243, 51561145021) and China Postdoctoral Science Foundation (Nos. 2019TQ0361 and 2020M672962).

REFERENCES

- (1) Englander, G. Property Rights and the Protection of Global Marine Resources. *Nat. Sustain.* **2019**, *2*, 981–987.
- (2) Sorensen, B. Renewable Energy: Commercial Hurdles to Wave Power. *Nature* **2017**, *543*, 491.
- (3) Wang, Z. L. New Wave Power. *Nature* **2017**, *542*, 159–160.
- (4) Scruggs, J.; Jacob, P. Engineering. Harvesting Ocean Wave Energy. *Science* **2009**, *323*, 1176–1178.
- (5) Zhang, C.; Liu, L.; Zhou, L.; Yin, X.; Wei, X.; Hu, Y.; Liu, Y.; Chen, S.; Wang, J.; Wang, Z. L. Self-Powered Sensor for Quantifying Ocean Surface Water Waves Based on Triboelectric Nanogenerator. *ACS Nano* **2020**, *14*, 7092–7100.
- (6) Kim, S. H.; Haines, C. S.; Li, N.; Kim, K. J.; Mun, T. J.; Choi, C.; Di, J.; Oh, Y. J.; Oviedo, J. P.; Bykova, J.; Fang, S.; Jiang, N.; Liu, Z.; Wang, R.; Kumar, P.; Qiao, R.; Priya, S.; Cho, K.; Kim, M.; Lucas, M. S.; et al. Harvesting Electrical Energy from Carbon Nanotube Yarn Twist. *Science* **2017**, *357*, 773–778.
- (7) Falnes, J. A Review of Wave-Energy Extraction. *Mar. Struct.* **2007**, *20*, 185–201.
- (8) Wu, Z.; Guo, H.; Ding, W.; Wang, Y. C.; Zhang, L.; Wang, Z. L. A Hybridized Triboelectric-Electromagnetic Water Wave Energy Harvester Based on a Magnetic Sphere. *ACS Nano* **2019**, *13*, 2349–2356.
- (9) Nie, J.; Wang, Z.; Ren, Z.; Li, S.; Chen, X.; Wang, Z. L. Power Generation from the Interaction of a Liquid Droplet and a Liquid Membrane. *Nat. Commun.* **2019**, *10*, 2264.
- (10) An, J.; Wang, Z.; Jiang, T.; Liang, X.; Wang, Z. L. Whirling-Folded Triboelectric Nanogenerator with High Average Power for Water Wave Energy Harvesting. *Adv. Funct. Mater.* **2019**, *29*, 1904867.
- (11) Liang, X.; Jiang, T.; Liu, G.; Xiao, T.; Xu, L.; Li, W.; Xi, F.; Zhang, C.; Wang, Z. L. Triboelectric Nanogenerator Networks Integrated with Power Management Module for Water Wave Energy Harvesting. *Adv. Funct. Mater.* **2019**, *29*, 1807241.
- (12) Liang, X.; Jiang, T.; Feng, Y.; Lu, P.; An, J.; Wang, Z. L. Triboelectric Nanogenerator Network Integrated with Charge Excitation Circuit for Effective Water Wave Energy Harvesting. *Adv. Energy Mater.* **2020**, *10*, 2002123.
- (13) Cheng, P.; Guo, H.; Wen, Z.; Zhang, C.; Yin, X.; Li, X.; Liu, D.; Song, W.; Sun, X.; Wang, J.; Wang, Z. L. Largely Enhanced Triboelectric Nanogenerator for Efficient Harvesting of Water Wave Energy by Soft Contacted Structure. *Nano Energy* **2019**, *57*, 432–439.
- (14) Zhang, C.; Zhao, Z.; Yang, O.; Yuan, W.; Zhou, L.; Yin, X.; Liu, L.; Li, Y.; Wang, Z. L.; Wang, J. Bionic-Fin-Structured Triboelectric Nanogenerators for Undersea Energy Harvesting. *Adv. Mater. Technol.* **2020**, *5*, 2000531.
- (15) Zhao, Z.; Dai, Y.; Liu, D.; Zhou, L.; Li, S.; Wang, Z. L.; Wang, J. Rationally Patterned Electrode of Direct-Current Triboelectric Nanogenerators for Ultrahigh Effective Surface Charge Density. *Nat. Commun.* **2020**, *11*, 6186.
- (16) Zhou, L.; Liu, D.; Wang, J.; Wang, Z. L. Triboelectric Nanogenerators: Fundamental Physics and Potential Applications. *Friction* **2020**, *8*, 481–506.
- (17) Zi, Y.; Guo, H.; Wen, Z.; Yeh, M. H.; Hu, C.; Wang, Z. L. Harvesting Low-Frequency (<5 Hz) Irregular Mechanical Energy: A Possible Killer Application of Triboelectric Nanogenerator. *ACS Nano* **2016**, *10*, 4797–4805.
- (18) Chen, J.; Yang, J.; Li, Z.; Fan, X.; Zi, Y.; Jing, Q.; Guo, H.; Wen, Z.; Pradel, K. C.; Niu, S.; Wang, Z. L. Networks of Triboelectric Nanogenerators for Harvesting Water Wave Energy: A Potential Approach toward Blue Energy. *ACS Nano* **2015**, *9*, 3324–3331.
- (19) Xi, Y.; Guo, H.; Zi, Y.; Li, X.; Wang, J.; Deng, J.; Li, S.; Hu, C.; Cao, X.; Wang, Z. L. Multifunctional TENG for Blue Energy Scavenging and Self-Powered Wind-Speed Sensor. *Adv. Energy Mater.* **2017**, *7*, 1602397.
- (20) Wang, H. S.; Jeong, C. K.; Seo, M. H.; Joe, D. J.; Han, J. H.; Yoon, J. B.; Lee, K. J. Performance-Enhanced Triboelectric Nanogenerator Enabled by Wafer-Scale Nanogrates of Multistep Pattern Downscaling. *Nano Energy* **2017**, *35*, 415–423.
- (21) Liu, D.; Zhou, L.; Wang, Z. L.; Wang, J. Triboelectric Nanogenerator: From Alternating Current to Direct Current. *iScience* **2021**, *24*, 102018.
- (22) Davey, R. J.; Williams-Seton, L.; Lieberman, H. F.; Blagden, N. Stabilizing a Solid-Solid Interface with a Molecular-Scale Adhesive. *Nature* **1999**, *402*, 797–799.
- (23) Liu, Y.; Liu, W.; Wang, Z.; He, W.; Tang, Q.; Xi, Y.; Wang, X.; Guo, H.; Hu, C. Quantifying Contact Status and the Air-Breakdown Model of Charge-Excitation Triboelectric Nanogenerators to Maximize Charge Density. *Nat. Commun.* **2020**, *11*, 1599.
- (24) Li, S.; Wang, S.; Zi, Y.; Wen, Z.; Lin, L.; Zhang, G.; Wang, Z. L. Largely Improving the Robustness and Lifetime of Triboelectric Nanogenerators through Automatic Transition between Contact and Noncontact Working States. *ACS Nano* **2015**, *9*, 7479–7487.
- (25) Wu, C.; Wang, A. C.; Ding, W.; Guo, H.; Wang, Z. L. Triboelectric Nanogenerator: A Foundation of the Energy for the New Era. *Adv. Energy Mater.* **2019**, *9*, 1802906.
- (26) Lin, Z.; Zhang, B.; Zou, H.; Wu, Z.; Guo, H.; Zhang, Y.; Yang, J.; Wang, Z. L. Rationally Designed Rotation Triboelectric Nanogenerators with Much Extended Lifetime and Durability. *Nano Energy* **2020**, *68*, 104378.
- (27) Lin, Z.; Zhang, B.; Guo, H.; Wu, Z.; Zou, H.; Yang, J.; Wang, Z. L. Super-Robust and Frequency-Multiplied Triboelectric Nanogenerator for Efficient Harvesting Water and Wind Energy. *Nano Energy* **2019**, *64*, 103908.
- (28) Wang, X.; Niu, S.; Yin, Y.; Yi, F.; You, Z.; Wang, Z. L. Triboelectric Nanogenerator Based on Fully Enclosed Rolling Spherical Structure for Harvesting Low-Frequency Water Wave Energy. *Adv. Energy Mater.* **2015**, *5*, 1501467.
- (29) Lin, S.; Xu, L.; Wang, A. C.; Wang, Z. L. Quantifying Electron-Transfer in Liquid-Solid Contact Electrification and the Formation of Electric Double-Layer. *Nat. Commun.* **2020**, *11*, 399.
- (30) Tang, W.; Chen, B.; Wang, Z. L. Recent Progress in Power Generation from Water/Liquid Droplet Interaction with Solid Surfaces. *Adv. Funct. Mater.* **2019**, *29*, 1901069.
- (31) Xu, W.; Zheng, H.; Liu, Y.; Zhou, X.; Zhang, C.; Song, Y.; Deng, X.; Leung, M.; Yang, Z.; Xu, R. X.; Wang, Z. L.; Zeng, X.; Wang, Z. A Droplet-Based Electricity Generator with High Instantaneous Power Density. *Nature* **2020**, *578*, 392–396.
- (32) Lin, Z. H.; Cheng, G.; Lee, S.; Pradel, K. C.; Wang, Z. L. Harvesting Water Drop Energy by a Sequential Contact-Electrification and Electrostatic-Induction Process. *Adv. Mater.* **2014**, *26*, 4690–4696.
- (33) Choi, D.; Kim, D.; Yoo, D.; Cha, K.; La, M.; Kim, D. Spontaneous Occurrence of Liquid-Solid Contact Electrification in Nature: Toward a Robust Triboelectric Nanogenerator Inspired by the Natural Lotus Leaf. *Nano Energy* **2017**, *36*, 250–259.
- (34) Wu, H.; Mendel, N.; van den Ende, D.; Zhou, G.; Mugele, F. Energy Harvesting from Drops Impacting onto Charged Surfaces. *Phys. Rev. Lett.* **2020**, *125*, 078301.
- (35) Zhang, B.; Wu, Z.; Lin, Z.; Guo, H.; Chun, F.; Yang, W.; Wang, Z. L. All-in-One 3D Acceleration Sensor Based on Coded Liquid-

Metal Triboelectric Nanogenerator for Vehicle Restraint System. *Mater. Today* **2021**, *43*, 37–44.

(36) Helseth, L. E.; Guo, X. D. Fluorinated Ethylene Propylene Thin Film for Water Droplet Energy Harvesting. *Renewable Energy* **2016**, *99*, 845–851.

(37) Pan, L.; Wang, J.; Wang, P.; Gao, R.; Wang, Y.-C.; Zhang, X.; Zou, J.-J.; Wang, Z. L. Liquid-FEP-Based U-Tube Triboelectric Nanogenerator for Harvesting Water-Wave Energy. *Nano Res.* **2018**, *11*, 4062–4073.

(38) Wu, H.; Wang, Z.; Zi, Y. Multi-Mode Water-Tube-Based Triboelectric Nanogenerator Designed for Low-Frequency Energy Harvesting with Ultrahigh Volumetric Charge Density. *Adv. Energy Mater.* **2021**, *11*, 2100038.

(39) Zhang, S. L.; Xu, M.; Zhang, C.; Wang, Y.-C.; Zou, H.; He, X.; Wang, Z.; Wang, Z. L. Rationally Designed Sea Snake Structure Based Triboelectric Nanogenerators for Effectively and Efficiently Harvesting Ocean Wave Energy with Minimized Water Screening Effect. *Nano Energy* **2018**, *48*, 421–429.

(40) Zhang, C.; Zhou, L.; Cheng, P.; Liu, D.; Zhang, C.; Li, X.; Li, S.; Wang, J.; Wang, Z. L. Bifilar-Pendulum Assisted Multilayer-Structured Triboelectric Nanogenerators for Wave Energy Harvesting. *Adv. Energy Mater.* **2021**, *11*, 2003616.

(41) Wang, Z. L. On Maxwell's Displacement Current for Energy and Sensors: The Origin of Nanogenerators. *Mater. Today* **2017**, *20*, 74–82.

(42) Chaplin, M. Theory vs Experiment: What is the Surface Charge of Water? *Water* **2009**, *1*, 1–28.

(43) Nie, J.; Ren, Z.; Xu, L.; Lin, S.; Zhan, F.; Chen, X.; Wang, Z. L. Probing Contact-Electrification-Induced Electron and Ion Transfers at a Liquid-Solid Interface. *Adv. Mater.* **2020**, *32*, 1905696.

(44) Jiang, P.; Zhang, L.; Guo, H.; Chen, C.; Wu, C.; Zhang, S.; Wang, Z. L. Signal Output of Triboelectric Nanogenerator at Oil-Water-Solid Multiphase Interfaces and Its Application for Dual-Signal Chemical Sensing. *Adv. Mater.* **2019**, *31*, 1902793.

(45) Wang, Z. L.; Wang, A. C. On the Origin of Contact-Electrification. *Mater. Today* **2019**, *30*, 34–51.

(46) Zhang, J.; Coote, M. L.; Ciampi, S. Electrostatics and Electrochemistry: Mechanism and Scope of Charge-Transfer Reactions on the Surface of Tribocharged Insulators. *J. Am. Chem. Soc.* **2021**, *143*, 3019–3032.

(47) Pan, S.; Zhang, Z. Fundamental Theories and Basic Principles of Triboelectric Effect: A Review. *Friction* **2019**, *7*, 2–17.

(48) Gennes, P. G. D.; Brochard-Wyart, F.; Quéré, D. *Capillarity and Wetting Phenomena: Drops, Bubbles, Pearls, Waves*; Springer, Science +Business Media: New York, 2004.

(49) You, J.; Shao, J.; He, Y.; Yun, F. F.; See, K. W.; Wang, Z. L.; Wang, X. High-Electrification Performance and Mechanism of a Water-Solid Mode Triboelectric Nanogenerator. *ACS Nano* **2021**, *15*, 8706–8714.

(50) Li, X.; Tao, J.; Wang, X.; Zhu, J.; Pan, C.; Wang, Z. L. Networks of High Performance Triboelectric Nanogenerators Based on Liquid-Solid Interface Contact Electrification for Harvesting Low-Frequency Blue Energy. *Adv. Energy Mater.* **2018**, *8*, 1800705.

(51) Zhang, J.; Rogers, F. J. M.; Darwish, N.; Gonçalves, V. R.; Vogel, Y. B.; Wang, F.; Gooding, J. J.; Peiris, M. C. R.; Jia, G.; Veder, J.-P.; Coote, M. L.; Ciampi, S. Electrochemistry on Tribocharged Polymers is Governed by the Stability of Surface Charges Rather than Charging Magnitude. *J. Am. Chem. Soc.* **2019**, *141*, 5863–5870.

(52) Li, S.; Nie, J.; Shi, Y.; Tao, X.; Wang, F.; Tian, J.; Lin, S.; Chen, X.; Wang, Z. L. Contributions of Different Functional Groups to Contact Electrification of Polymers. *Adv. Mater.* **2020**, *32*, 2001307.

(53) Zou, H.; Zhang, Y.; Guo, L.; Wang, P.; He, X.; Dai, G.; Zheng, H.; Chen, C.; Wang, A. C.; Xu, C.; Wang, Z. L. Quantifying the Triboelectric Series. *Nat. Commun.* **2019**, *10*, 1427.

(54) Cao, S.; Zhang, H.; Cui, X.; Yuan, Z.; Ding, J.; Sang, S. Fully-Enclosed Metal Electrode-Free Triboelectric Nanogenerator for Scavenging Vibrational Energy and Alternatively Powering Personal Electronics. *Adv. Eng. Mater.* **2019**, *21*, 1800823.